Journal of Theoretical and Applied Mechanics, Sofia, 2008, vol. 38, Nos 1–2, pp. 81–100

SHEAR LOCALISATION IN THICK-WALLED CYLINDERS UNDER INTERNAL PRESSURE BASED ON GRADIENT ELASTOPLASTICITY*

A. Zervos
School of Civil Engineering and the Environment, University of Southampton, SO17 1BJ, UK,
e-mail: az@soton.ac.uk

P. Papanastasiou
Department of Civil and Environmental Engineering, University of Cyprus, P.O.Box 20537 Nicosia, 1678, Cyprus,
e-mail: panospap@ucy.ac.cy

I. Vardoulakis
Section of Mechanics, National Technical University of Athens, Zografou 157 73, Greece,
e-mail: I.Vardoulakis@mechan.ntua.gr

[Received 17 September. Accepted 25 February 2008]

Abstract. We studied failure of thick-walled cylinders under external confinement and internal pressurisation. The material is assumed to be pressure-sensitive with dilatant and strain-softening response. The analysis was carried out using Gradient Elastoplasticity, a higher order theory developed to regularise the ill-posed problem caused by material strain-softening. In this theory the stress increment is related to both the strain increment and its Laplacian. The gradient terms in the constitutive equations introduce an extra parameter of internal length related to material micro-structure, allowing robust modelling of the post-peak material behaviour. The governing equations were solved numerically with the displacement finite element formulation, using C^1-continuity elements. Numerical results show that at a critical loading threshold the initial axisymmetry of deformation breaks spontaneously and an instability of finite wavenumber develops. With increasing pressurisation, a curved shear-band of finite thickness forms and propagates progressively towards the outer boundary. For high confining pressures this mode of

*The authors are grateful to Schlumberger Cambridge Research for supporting this research. A. Zervos also acknowledges the support of the School of Civil Engineering and the Environment, University of Southampton.

shear failure is more critical than the trivial tensile failure mode. Practical applications can be found in wellbore stability and hydraulic fracturing in petroleum engineering, and in pile driving design and the interpretation of pressuremeter and penetrometer tests in geotechnical engineering.
KEY WORDS: gradient elastoplasticity, gradient plasticity, cavity expansion, shear localisation, strain softening, finite elements.

1. Introduction

The problem of cylindrical cavity expansion is of significant interest in geotechnical, petroleum and mining engineering. In geotechnical engineering the analysis of an internally pressurised cavity is essential in interpreting pressuremeter and penetrometer tests and in modelling the process of foundation-pile driving [1, 2]. In this paper the study of cavity pressurisation is motivated by two applications in petroleum engineering related to wellbore stability and hydraulic fracturing.

In petroleum engineering, a wellbore is supported temporarily during drilling by a mud-column to prevent the costly occurrence of wellbore collapse. The optimal mud-density lies within an operating window which can be derived using mathematical models. The lower bound of this window is usually designed to prevent compressive collapse. The upper bound is designed mainly to avoid unwanted fracturing which may result in expensive mud-losses. In many fields around the world the mud-window is quite narrow, due to other considerations as well, requiring determination with more accurate models. The second application is related to hydraulic fracturing, which is a technique used to stimulate oil and gas reservoirs by inducing fractures in the formation and then propagating them by the injection of a high viscosity fluid [3]. A useful information in the design of hydraulic fracturing is the breakdown pressure, i.e. the pressure level at which the formation breaks down and the fracture is initiated. In both applications, the upper bound of the mud-density or the breakdown pressure can be determined assuming that the material around the wellbore remains elastic and a tensile crack is initiated when the hoop stress exceeds the tensile strength of the rock. This condition is expressed by the equation of the stress concentration around the wellbore

$$P_b = 3\sigma_h + \sigma_H + T, \tag{1}$$

where P_b is the breakdown pressure, T is the tensile strength of the rock and σ_H and σ_h are the maximum and minimum horizontal insitu stresses, respectively [4].

Equation (1) appears to yield reasonable results in strong formations. This observation is also supported by experimental evidence from internally pressurised thick–walled cylinders, suggesting that equation (1) is indeed valid in the elastic regime. In the plastic regime, however, Mohr–Coulomb elastoplastic analysis predicts higher breakdown pressures than the ones observed [5]. For sufficiently high confining pressures, elastoplastic analysis predicts that a tensile state of stress during pressurisation cannot be achieved, although significantly lower breakdown pressures were observed in the experiments. In addition, if the formation is weakly consolidated or unconsolidated, it could be suggested that the observed breakdown pressure should be related not with the initiation of a fracture, but with the limit pressure, i.e. the value of the internal pressure at which the radius of the cavity grows uncontrollably.

Here we investigate fracture initiation in weak materials by examining the possibility that tensile failure is preceded by the onset of shear localisation. A theory with microstructure is utilised, called Gradient Elastoplasticity, which has been proven capable of modelling localisation of deformation in a robust way in other geomechanics problems [6, 7, 8]. It will be shown that, during cavity pressurisation, it is possible for the axisymmetry of deformation to break spontaneously at a loading threshold, leading to deformation localisation in shearbands. Lower breakdown pressures can then be explained if the pressurising fluid is considered to penetrate into these shear zones, causing them to propagate further in a tensile mode.

In the following we briefly review the basics of the theory of Gradient Elastoplasticity in Section 2. In Section 3 the problem of axisymmetric cavity expansion is considered, and bifurcation analysis is used to examine the stability of the cavity. Finite element analysis is employed to determine the internal pressure that causes instability, and the geometrical characteristics of the corresponding instability mode for different cylinder sizes. In Section 4 a more general numerical treatment is presented, able to capture the inception of instabilities and the resulting localised failure mechanisms in the post-bifurcation regime. Numerical results are presented and compared to the predictions of bifurcation analysis. Finally, some conclusions are drawn and discussed in Section 5.

2. Gradient Elastoplasticity

2.1. Governing equations

We consider a decomposition of the total strain rate $\dot{\epsilon}_{ij}$ into an elastic part $\dot{\epsilon}^e_{ij}$ and a plastic part $\dot{\epsilon}^p_{ij}$, as:

$$\dot{\epsilon}_{ij} = \dot{\epsilon}^e_{ij} + \dot{\epsilon}^p_{ij}, \tag{2}$$

and define the total (equilibrium) stress rate $\dot{\sigma}_{ij}$ in terms of the elastic strain rate and its Laplacian:

$$\dot{\sigma}_{ij} = C^e_{ijkl}\left(\dot{\epsilon}^e_{kl} - l_e^2\nabla^2\dot{\epsilon}^e_{kl}\right). \tag{3}$$

In the above C^e_{ijkl} is the tensor of elastic moduli and l_e is a material length parameter, termed the *elastic material length*.

The yield condition is defined as $F(\tau_{ij}, \psi) = 0$ where F is the yield function. The plastic strain rate is considered normal to a plastic potential function $Q(\tau_{ij}, \psi)$:

$$\dot{\epsilon}^p_{ij} = \dot{\psi}\frac{\partial Q}{\partial \tau_{ij}}, \tag{4}$$

where $\dot{\psi}$ is the plastic multiplier. Setting $Q \equiv F$ leads to the special case of associative plasticity. The yield function F and the plastic potential Q are both assumed to depend on a reduced stresses τ_{ij} and a hardening/softening parameter ψ. The reduced stress rate is defined as:

$$\dot{\tau}_{ij} = \dot{\sigma}_{ij} - \dot{\alpha}_{ij}, \tag{5}$$

where α_{ij} is a back stress, evolving in the course of plastic straining according to the following law:

$$\dot{\alpha}_{ij} = -C^e_{ijkl} l_p^2 \nabla^2 \dot{\epsilon}^p_{kl}. \tag{6}$$

The scalar parameter l_p is termed the *plastic material length*. The physical meaning of the above law is that back stresses develop only where the deformation becomes sufficiently inhomogeneous, allowing for a region around a material point to contribute to its strength, and thus countering the destabilising effect of material softening.

To determine the plastic strain increments corresponding to a load increment, the value of the plastic multiplier $\dot{\psi}$ needs to be determined first. This is done through the consistency condition, which ensures that the stress state remains on the yield surface during plastic deformation:

$$F(\tau_{ij}, \psi) = 0, \qquad \dot{F}(\tau_{ij}, \psi) = \frac{\partial F}{\partial \tau_{ij}}\dot{\tau}_{ij} + \frac{\partial F}{\partial \psi}\dot{\psi} = 0. \tag{7}$$

Combining equations (2) to (7) and neglecting terms of order higher than second yields the following equation for the plastic multiplier:

$$\left[1 - \frac{H_0}{H}\left(l_e^2 + l_p^2\right)\nabla^2\right]\dot{\psi} = \frac{1}{H}\frac{\partial F}{\partial \tau_{ij}} C^e_{ijkl}\left(\dot{\epsilon}_{kl} - l_e^2\nabla^2\dot{\epsilon}_{kl}\right), \tag{8}$$

$$H = H_0 + H_t,$$

$$H_0 = \frac{\partial F}{\partial \tau_{ij}} C^e_{ijkl} \frac{\partial Q}{\partial \tau_{kl}},$$

$$H_t = -\frac{\partial F}{\partial \psi}.$$

Unlike classical plasticity, where the consistency condition is an algebraic equation, equation (8) is a differential equation that would have to be discretised. Nevertheless, this can be avoided by producing an approximate analytical solution, as detailed in [9] and [6]. This yields:

$$\dot{\psi} = \frac{1}{H}\frac{\partial F}{\partial \tau_{ij}} C^e_{ijkl}\left(\dot{\epsilon}_{kl} + l_c^2\nabla^2\dot{\epsilon}_{kl}\right), \tag{9}$$

where

$$l_c^2 = \frac{H_0}{H} l_p^2 - \frac{H_t}{H} l_e^2 > 0. \tag{10}$$

To facilitate the numerical implementation, total stress and back stress rates are written in terms of total strain rates as:

$$\dot{\sigma}_{ij} = C^{ep}_{ijkl}\dot{\epsilon}_{kl} - C^m_{ijkl}\nabla^2\dot{\epsilon}_{kl}, \tag{11}$$

$$\dot{\alpha}_{ij} = -l_p^2 C^p_{ijkl}\nabla^2\dot{\epsilon}_{kl}, \tag{12}$$

where C^p_{ijkl} is the *plastic stiffness matrix* of classical plasticity

$$C^p_{ijkl} = \frac{<1>}{H} C^e_{ijmn}\frac{\partial Q}{\partial \tau_{mn}}\frac{\partial F}{\partial \tau_{st}} C^e_{stkl}, \tag{13}$$

and $<>$ are the McAuley brackets defined by

$$<1> = \begin{cases} 1, \text{ if } F = 0 \text{ and } \dot{\psi} \geq 0, \\ 0, \text{ if } F < 0, \text{ or } F = 0 \text{ and } \dot{\psi} < 0. \end{cases} \tag{14}$$

$C^{ep}_{ijkl} = C^{e}_{ijkl} - C^{p}_{ijkl}$ is the usual *elastoplastic stiffness matrix* and, finally, $C^{m}_{ijkl} = l_e^2 C^{ep}_{ijkl} + l_c^2 C^{p}_{ijkl}$ is a stiffness matrix for the second gradient terms.

We note that at the limit of $l_e = 0$ the above equations degenerate to the gradient plasticity model presented in [10], [11] and [12]. Furthermore, for $l_e = l_p = 0$ the classical theory of elastoplasticity is recovered.

2.2. Principle of virtual work

The ideas presented above can be re-interpreted within Mindlin's framework for continua with microstructure [13], which then readily provides the expressions for the internal and external virtual work. Following the terminology of [13] and [10], we can rewrite the total stress rate as $\dot{\sigma}_{ij} = \dot{\sigma}^{(0)}_{ij} + \dot{\sigma}^{(2)}_{ij} = (C^{ep}_{ijkl}\dot{\epsilon}_{kl}) + (-C^{m}_{ijkl}\nabla^2\dot{\epsilon}_{kl})$. Here $\dot{\sigma}^{(0)}_{ij}$ is the *Cauchy stress rate*, which is identified as the constitutive stress rate tensor of classical elastoplasticity and it relates to the strain rate, while the second term is a *relative stress rate* $\dot{\sigma}^{(2)}_{ij}$, which relates to the Laplacian of the strain rate. It is further postulated that the relative stress is equilibrated by a *double stress rate* $\dot{m}_{kij}$, energy conjugate to the strain gradient $\dot{\epsilon}_{ij,k}$. The double stress rate should be such that

$$\dot{\sigma}^{(2)}_{ij} + \dot{m}_{kij,k} = 0 \longrightarrow \dot{m}_{kij} = C^{m}_{ijmn}\dot{\epsilon}_{mn,k}. \tag{15}$$

The virtual work of internal forces can now be written as:

$$\delta\dot{W}_{int} = \int_V \left(\sigma^{(0)}_{ij}\delta\dot{\epsilon}_{ij} + m_{kij}\delta\dot{\epsilon}_{ij,k}\right) dV. \tag{16}$$

To calculate the work of external forces, we split the boundary S in two parts, S_u and S_σ. Dirichlet boundary conditions are applied at S_u. We note that, due to the presence of strain gradients, Dirichlet boundary conditions can contain restrictions on the displacement as well as its normal derivative at the boundary. Neumann boundary conditions are applied at S_σ. In the absence of body forces, the external work can be written as:

$$\delta\dot{W}_{ext} = \int_{S_\sigma} \left(t_i\delta\dot{v}_i + \mu_i n_k \delta\dot{v}_{i,k}\right) dS, \tag{17}$$

where t_i is the applied traction vector, μ_i is the applied double traction vector, n_i is the unit normal to S_σ and $\delta\dot{v}_i$ is the virtual displacement rate vector on S_σ.

The principle of virtual work can then be written as:

$$\int_V \left(\sigma_{ij}^{(0)} \delta\dot{\epsilon}_{ij} + m_{kij}\delta\dot{\epsilon}_{ij,k}\right) dV = \int_{S_\sigma} \left(t_i \delta\dot{v}_i + \mu_i n_k \delta\dot{v}_{i,k}\right) dS. \tag{18}$$

The above expression, which is equivalent to the conditions of static equilibrium, will be used in the following as the basis for the development of numerical solutions of axisymmetric and plane strain boundary value problems.

We note that the term μ_i of the right-hand side of equation (18) is a higher-order force-like quantity known as *double force*, which corresponds to a boundary condition on the projection of the double stress. This is conceptually similar to the applied traction being a boundary condition on the projection of the Cauchy stress tensor. A double force corresponds to a pair of co-linear and opposite forces, and works on the normal-to-the-boundary derivative of the displacement field. Double forces can be easily accommodated within a numerical framework, e.g. one based on the finite element method, in the same way as usual tractions, the only difference being that they work on the derivative of the displacement rather than the displacement itself.

3. Inception of shear failure during uniform cavity expansion

3.1. Geometry and boundary conditions

We consider the thick-walled cylinder shown in Fig. 1(a), with internal radius R_i and external radius R_e, under plane strain conditions. A uniform pressure p_i is applied in the cavity, and a uniform pressure p_e is applied at the external boundary. We examine the particular case where loading of the cylinder takes place in two stages: First, p_i and p_e are increased simultaneously from zero to some predetermined value of confinement p_0. Subsequently, p_i is further increased to failure under constant p_e.

In the problem described above both the geometry and the loads are axisymmetric, hence the deformation can also be expected to be axisymmetric. Depending on the stress level and the strength of the material, it is normally considered that the cylinder may fail in one of two different ways: If the hoop stress at the cavity wall becomes tensile and greater than the tensile strength of the material, the cylinder will fail due to the propagation of a tensile fracture. Alternatively, if due to plasticity and high confinement a tensile stress cannot develop, the cylinder will eventually fail when the plastic zone spreads adequately to allow uncontrollable uniform expansion of the cavity. The corresponding internal pressure is referred to as the "limit pressure" in the context of geotechnical engineering.

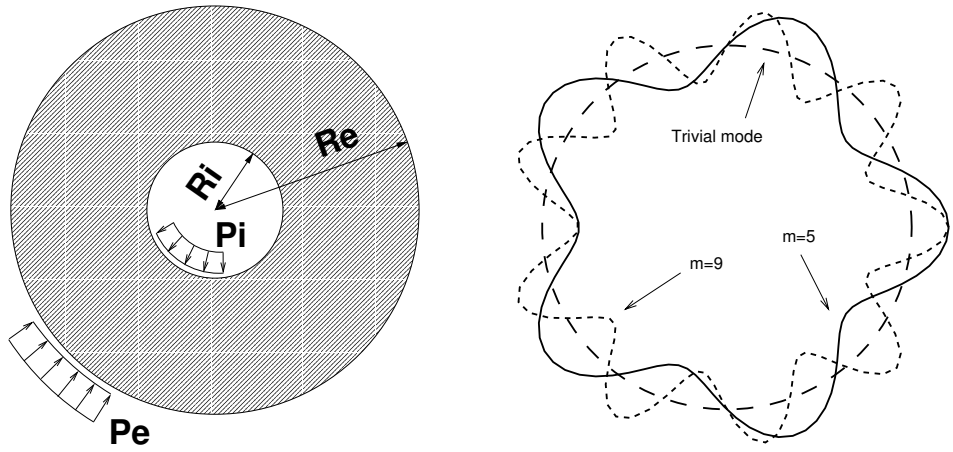

(a) Geometry and loading (b) Trivial vs non-trivial modes of deformation

Fig. 1. Geometry, loading and deformation modes of a thick-walled cylinder

Here we investigate the possibility that shear failure may precede both tensile failure and the attainment of limit pressure. This is possible if, at some stress level, the cavity becomes unstable and warps, leading to stress redistribution which would promote localised shear failure. In the remainder of this section, we first present a numerical treatment for the problem of uniform cavity expansion. Subsequently the conditions for the development of instabilities are discussed, a numerical approach for their detection is developed and some numerical results are presented.

3.2. Uniform cavity expansion

For the thick-walled cylinder of Fig. 1(a), we consider an infinitesimal increase δp_i of the internal pressure and examine the resulting deformation of the cavity. The applied double force at the boundary is taken to be zero.

One possibility is that the cavity will expand uniformly and deformations will remain axisymmetric. This will be called in the following the *trivial deformation path*. If written in cylindrical co-ordinates the boundary value problem is one-dimensional, as $u_r(r)$, $u_\theta = 0$, and $(\partial \cdot / \partial\theta) = 0$, so in a finite element formulation only the radial displacement u_r needs to be discretised. Such a formulation is sketched briefly in the following, based on the algorithms presented in [6].

We consider the interpolation $u_r = \boldsymbol{N} \cdot \widehat{\boldsymbol{u}}$, where $\boldsymbol{N}$ a matrix of shape functions and $\widehat{\boldsymbol{u}}$ a vector of appropriate degrees of freedom. Strains and strain gradients can then be written in vector form, as $\boldsymbol{\epsilon} = \boldsymbol{B_1} \cdot \widehat{\boldsymbol{u}}$ and $\boldsymbol{\kappa} = \boldsymbol{B_2} \cdot \widehat{\boldsymbol{u}}$

respectively, where the matrices $\boldsymbol{B_1}$ and $\boldsymbol{B_2}$ contain appropriate combinations of $\boldsymbol{N}$ and their first and second derivatives with respect to r. Cauchy stress and double stress increments can also be written in vector form and linked to strain and strain gradient increments, as $\dot{\boldsymbol{\sigma}}^{(\mathbf{0})} = \boldsymbol{C^{ep}} \cdot \dot{\boldsymbol{\epsilon}}$ and $\dot{\boldsymbol{m}} = \boldsymbol{C^{m}} \cdot \dot{\boldsymbol{\kappa}}$ respectively.

Substitution of the above into equation (18) yields the weak form of the boundary value problem:

$$\int_{R_i}^{R_e} \left(\boldsymbol{B_1^T C^{ep} B_1} + \boldsymbol{B_2^T C^{m} B_2}\right) r dr \cdot \dot{\hat{\boldsymbol{u}}} = \boldsymbol{K_t} \cdot \dot{\hat{\boldsymbol{u}}} = \dot{\boldsymbol{f}}, \tag{19}$$

where $\dot{\boldsymbol{f}}$ is the load vector corresponding to δp_i and $\boldsymbol{K_t}$ is the stiffness matrix corresponding to the trivial deformation path. Solving equation (19) yields the deformation corresponding to axisymmetric expansion.

We note that, due to the strain gradients in equations (18) and (19), the interpolation used should guarantee continuity of strains, i.e. a finite element guaranteeing C^1-continuity should be used. Such an element is the cubic Hermite element, which was adopted here. It has two nodes, and employs u_r and $u_{r,r}$ as degrees of freedom at each node. The element and its shape functions are shown in Fig. 2.

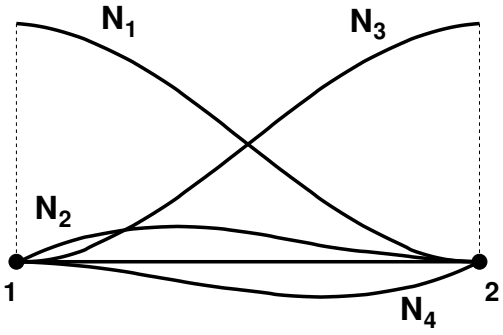

Fig. 2. The cubic Hermite element and its shape functions

3.3. Non-uniform cavity warping

We now return to the thick-walled cylinder of Fig. 1(a), and again we consider an infinitesimal increase δp_i of the internal pressure. Apart from axisymmetric expansion of the cavity, which was treated above, a second possibility is that the cavity will lose its axisymmetric shape and warp. Mathematically this is possible if, in addition to the trivial deformation mode, a

non-trivial, non-axisymmetric solution exists, which fulfills the homogeneous boundary condition $\delta p_i = 0$. Then an equilibrium bifurcation is said to be taking place. Here we consider non-trivial incremental solutions for the displacement field, of the form $\dot{u}_r = u_r^0(r) \cdot \cos(m\theta)$ and $\dot{u}_\theta = u_\theta^0(r) \cdot \sin(m\theta)$. The integer $m > 0$ is a wavenumber determining the wavelength of the bifurcation mode. Examples of the shape of these modes at the cavity wall are compared to the trivial mode in Fig. 1(b).

In a finite element formulation, both u_r and u_θ now need to be discretised. In line with the previous subsection, we consider an interpolation $\boldsymbol{u} = \{u_r,\ u_\theta\} = \boldsymbol{N} \cdot \widehat{\boldsymbol{u}}$, where $\boldsymbol{N}$ a matrix of shape functions and $\widehat{\boldsymbol{u}}$ a vector of appropriate degrees of freedom. Strains and strain gradients become $\boldsymbol{\epsilon} = \boldsymbol{B_{1,n}} \cdot \widehat{\boldsymbol{u}}$ and $\boldsymbol{\kappa} = \boldsymbol{B_{2,n}} \cdot \widehat{\boldsymbol{u}}$ respectively, where the matrices $\boldsymbol{B_{1,n}}(m)$ and $\boldsymbol{B_{2,n}}(m)$ contain combinations of $\boldsymbol{N}$ and their first and second derivatives with respect to r, but are also functions of the wavenumber m.

Since solutions are sought for $\delta p_i = 0$, substitution of the above into equation (18) yields:

$$\int_{R_i}^{R_e} \left(\boldsymbol{B_{1,n}^T C^{ep} B_{1,n}} + \boldsymbol{B_{2,n}^T C^m B_{2,n}}\right) r dr \cdot \dot{\widehat{\boldsymbol{u}}} = \boldsymbol{K_{nt}} \cdot \dot{\widehat{\boldsymbol{u}}} = \boldsymbol{0}. \tag{20}$$

Again C^1 interpolation is required, so cubic Hermite elements are used to interpolate both u_r^0 and u_θ^0. The nodal degrees of freedom employed are u_r^0, $u_{r,r}^0$, u_θ^0 and $u_{\theta,r}^0$.

The $\boldsymbol{B}$-matrices in equation (20) depend on the wavenumber m, resulting to a different stiffness matrix $\boldsymbol{K_{nt}}(m)$ for each particular non-trivial deformation mode. Warping of the cavity with wavenumber m is possible only if equation (20) has non-zero solutions, i.e. only if $\det\{\boldsymbol{K_{nt}}(m)\} = 0$. Thus, the criterion for non-uniform warping of the cavity at internal pressure p_i is that $\det\{\boldsymbol{K_{nt}}(m)\} = 0$ at that pressure, for at least one value of m; warping with wavenumber m is then possible.

3.4. Numerical results

As an example we model internal pressurisation of four thick-walled cylinders of a weak sandstone, with $R_i = 5, 10, 20$ and 40 cm, and $R_e = 6R_i$. The material behaviour is described by the Mohr-Coulomb failure criterion:

$$F = m\tau_1 - \tau_3 - \sigma_c = 0, \tag{21}$$

where $m = (1+\sin\phi)/(1-\sin\phi)$ is the friction coefficient and $\sigma_c = (2c\cos\phi)/(1-\sin\phi)$ is the *equivalent stress*; ϕ is the angle of internal friction and c is the material cohesion. The material parameters were calibrated from triaxial tests on Castlegate sandstone. The elastic constants were found to be $E = 8100$ MPa and $\nu = 0.35$. The friction angle is considered constant, with a value $\phi = 32.54^\circ$ and an associated flow-rule is assumed. The hardening/softening behaviour is defined through the equivalent stress $\sigma_c(\epsilon_p)$, taken to evolve according to the hyperbolic law:

$$\sigma_c(\epsilon_p) = \sigma_{c,0} + \frac{(1 - C_0\epsilon_p)\epsilon_p}{C_1 + C_2\epsilon_p}, \tag{22}$$

where $C_1 = 1.323 \cdot 10^{-5}$ and $C_2 = 6.1271 \cdot 10^{-2}$ are calibration constants. $\sigma_{c,0} = 25$ MPa is a conventional threshold value of the equivalent stress defining the state of initial yield. The constant C_0 is an open parameter controlling the rate of softening; it is taken to be $C_0 = 70$. The plastic material length is set to $l_p = 0.2$ mm, equal to the mean grain diameter of the Castlegate sandstone.

The elastic material length could in principle be taken zero, as linear elasticity represents satisfactorily the elastic behaviour of the sandstone at hand. However, the value $l_e = 0$ would lead to a change of the order of the governing equations when crossing the internal elastoplastic boundary, which in turn would introduce the need for tracking the internal elastoplastic boundary and applying boundary conditions on it. This is an unwelcome complication that is very difficult to treat numerically. Here we choose to use a finite value $l_e = l_p/10 = 0.02$ mm, to ensure that the order of the governing equations remains the same. This value is small enough to ensure that gradient effects in elasticity are negligible [7].

Both an internal pressure p_i and an external pressure p_e are applied: first the cylinders are loaded with $p_i = p_e = 30$ MPa and subsequently p_i is increased under constant p_e. It was found that converged results can be obtained using a mesh of 40 elements; the mesh is refined close to the hole using a geometric progression with ratio 1.22, to capture accurately the stress concentration.

The load is increased incrementally and equation (19) is solved to calculate the deformations corresponding to the trivial path. After each increment, $\det\{\boldsymbol{K_{nt}}(m)\}$ is calculated for all $1 \leq m \leq 100$ using equation (20). Initially, for all values of m it is $\det\{\boldsymbol{K_{nt}}(m)\} > 0$. If, at a given stress level, $\det\{\boldsymbol{K_{nt}}(m)\} < 0$ for some value of m, warping according to mode m is possible during the current load increment. The lowest internal pressure for which

$\det\{\boldsymbol{K_{nt}}(m)\} < 0$ is the *bifurcation pressure* for that mode.

In Figure 3(a) the bifurcation pressure is plotted as a function of m for the different cylinder sizes. For each cylinder size, the minimum pressure for which a non-trivial solution is possible is called the *critical bifurcation pressure*, and its corresponding mode the *critical bifurcation mode*. When this pressure is reached, the expanding cavity becomes unstable and warps. It has been shown experimentally that a similar process takes place in expanding cavities in sands, giving rise to deformation localisation in thin shearbands [14].

It is also worth noting that the critical bifurcation mode is finite and it increases with the size of the cylinder. This phenomenon of wavenumber selection is the result of incorporating microstructure in the constitutive equations, and has also been demonstrated for contracting cavities [15, 7]. Within the framework of classical Elastoplasticity, where material microstructure is ignored, wavenumber selection does not take place. As a result, bifurcation analyses like the above predict instabilities of infinite wavenumber, which can be interpreted as surface instabilities [16].

In Figure 3(b) a plot of internal pressure vs dimensionless hole deformation for the trivial mode of axisymmetric expansion is presented. This plot is common for all the cylinder sizes examined. The critical bifurcation pressure for each cylinder is marked with a point along the trivial path, showing clearly that smaller holes are predicted to warp at higher pressure, and thus exhibit higher strength. This scale effect is similar to that observed in experiments of cavities under external load [17], where smaller cavities are shown to fail under higher pressure.

It is noted that, due to the high confinement used and the development of a plastic zone around the hole, no tensile hoop stress developed in the course of the analyses reported. Hence none of the cylinders is predicted to fail due to the propagation of tensile fractures. In addition, Fig. 3(b) shows that for all cylinders warping is possible well before reaching limit pressure, which is identified as the pressure to which the trivial path asymptotically tends.

As already mentioned, warping would lead to stress redistribution around the cavity, promoting the progressive development of localised shear failure mechanisms. Capturing progressive failure in detail, however, is beyond the scope of the numerical treatments presented in this section. Two-dimensional analyses are needed for that, where the cross-sectional geometry of the cylinders is modelled in detail. To investigate this issue further, a corresponding finite element formulation is presented in the next section along with some numerical results.

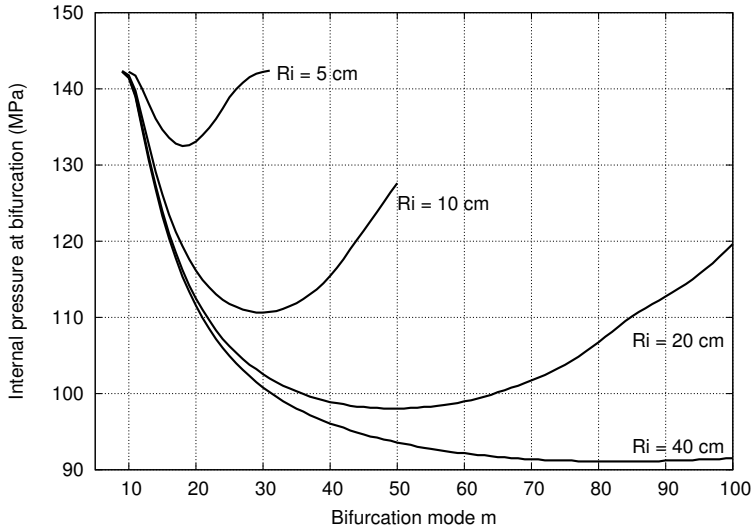

(a) Bifurcation pressure vs bifurcation mode

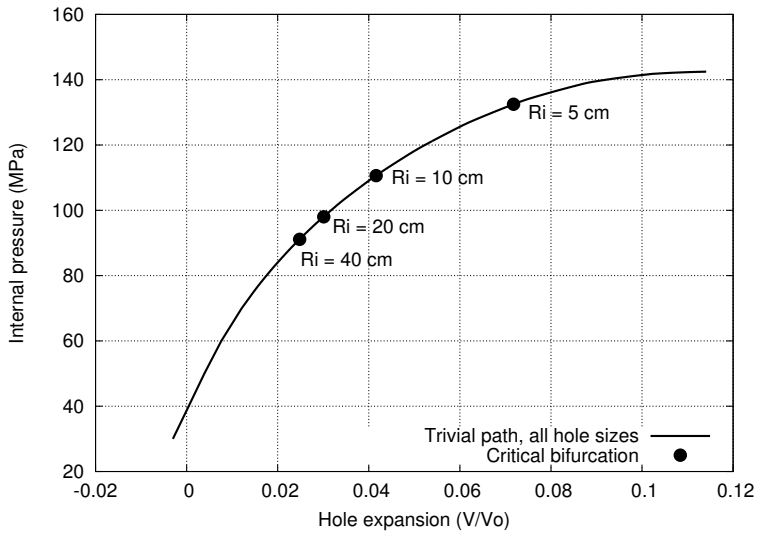

(b) Trivial path and critical bifurcation pressure

Fig. 3. Results for the different cylinder sizes

4. Progressive shear failure during cavity expansion

4.1. Finite element formulation for two-dimensional problems

We consider again the problem of Fig. 1(a) in plane strain conditions. To each material point (x, y) we can attach a displacement vector $\boldsymbol{u} = \{u_x, u_y\}$. As in the previous section, we assume an interpolation $\boldsymbol{u} = \boldsymbol{N} \cdot \widehat{\boldsymbol{u}}$, where $\boldsymbol{N}$ and $\widehat{\boldsymbol{u}}$ are the shape functions and degrees of freedom respectively, strains are $\boldsymbol{\epsilon} = \boldsymbol{B_1} \cdot \widehat{\boldsymbol{u}}$ and strain gradients $\boldsymbol{\kappa} = \boldsymbol{B_2} \cdot \widehat{\boldsymbol{u}}$. The matrices $\boldsymbol{B_1}$ and $\boldsymbol{B_2}$ now contain first and second derivatives, respectively, of the shape functions. Cauchy stress and double stress increments are also written in vector form and linked to strain and strain gradient increments as in the previous section; details of the algorithms and the exact form of the relevant matrices can be found in [6]. Finally, substitution into equation (18) yields the weak form of the boundary value problem as:

$$\int_V \left(\boldsymbol{B_1^T C^{ep} B_1} + \boldsymbol{B_2^T C^m B_2}\right) \cdot \dot{\widehat{\boldsymbol{u}}} = \boldsymbol{K} \cdot \dot{\widehat{\boldsymbol{u}}} = \dot{\boldsymbol{f}}, \tag{23}$$

where $\boldsymbol{K}$ is the stiffness matrix.

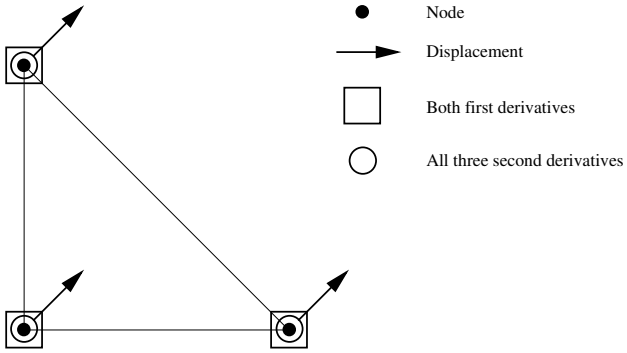

Fig. 4. The C^1 triangle with 18 degrees of freedom

The finite element we use is the three-noded C^1 triangle with 18 degrees of freedom for each interpolated field, shown in Fig. 4. This element is a constrained version of the six-noded C^1 triangle originally presented in reference [18]. The displacement field varies as a complete quintic inside the element, while its normal derivative along the element edges is constrained to be cubic. Since the first and second derivatives at the corners suffice to define uniquely a cubic polynomial along each edge, derivatives are continuous across elements. The total degrees of freedom of the element are $2(3 \cdot 6) = 36$, and

its shape functions were derived in analytical form in reference [19]. The element is integrated using the standard 13-point Gauss quadrature scheme for the triangle, which is sufficiently accurate to ensure convergence [6].

4.2. Numerical results

As an example we model internal pressurisation of the thick-walled cylinder with $R_i = 10$ cm, presented in the previous section. The same material model and material parameters as in the previous section are used, and the same two-stage loading is applied assuming zero double force at the boundary. To eliminate rigid body modes, four nodes on the outer surface of the cylinder are constrained: the two nodes at $(0, \pm R_e)$ are constrained so that $u_x = 0$, and the two nodes at $(\pm R_e, 0)$ are constrained so that $u_y = 0$. A mesh with 17 nodes in the radial direction and 160 around the circumference is used. A geometric progression is employed in the radial direction to produce a finer mesh near the hole. The mesh consists of 5440 elements with 2720 nodes, giving a total of 32640 degrees of freedom. Extensive mesh-sensitivity studies carried out previously showed that the above mesh density suffices to provide converged results for the chosen values of the material parameters [6, 7, 8]. A detail of the mesh near the hole is shown in Fig. 5(a).

During the first stage of loading, when $p_i = p_e$, no yielding occurs. In the second stage, as p_i increases, the material near the hole yields following the hardening branch initially, and eventually entering the softening regime. Deformation is initially axisymmetric, as shown by the contour plot of Fig. 5(b) which represents the radial displacement increment.

As the internal pressure approaches $p_i = 110$ MPa, axisymmetry of the deformation breaks spontaneously and the radial displacement increment in the vicinity of the hole assumes the sinusoidal form shown in Fig. 5(c). Both the wavenumber of the instability, which is 31, and the load level at which it appears, correspond closely to the ones predicted for this cylinder using bifurcation analysis (c.f. Fig. 3(a)). This provides confidence that the numerical results obtained are not spurious, but correspond to a valid, non-trivial bifurcated solution. It is also further evidence that the mesh employed is indeed adequate for providing converged numerical resuls.

After the manifestation of the instability, some regions of the material near the cavity unload elastically. With increasing load the unloading areas grow in size and coalesce, while deformation localises into thin bands of softening material that continue to shear. These shearbands are shown in Fig. 5(d) with black points. In the same figure, gray points show material still in the hardening regime while, for clarity, virgin-elastic and elastically unloading ma-

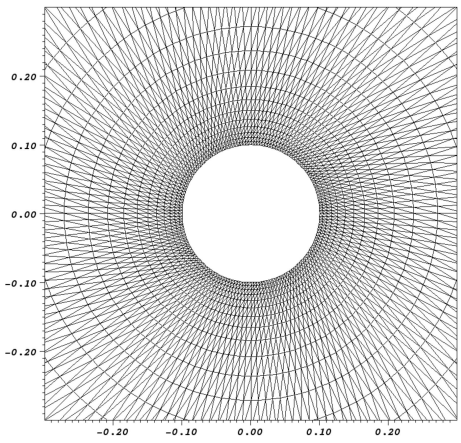

(a) Mesh detail near the hole

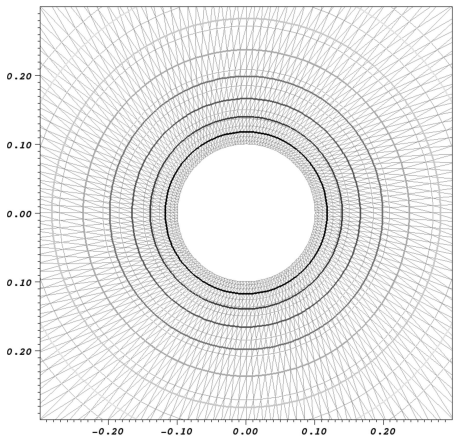

(b) Material state and displacement increment

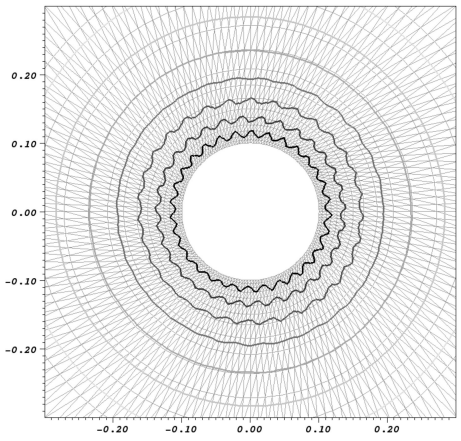

(c) Radial displ. increment at bifurcation

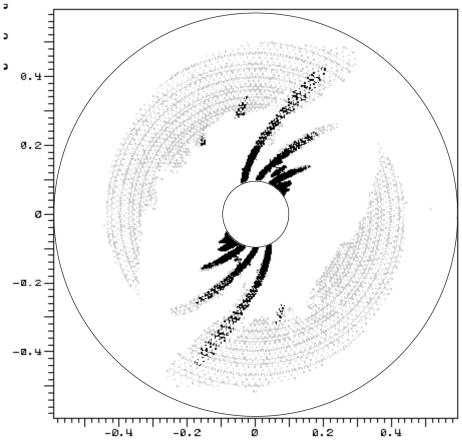

(d) Final material state

Fig. 5. Results for the $R_i = 10$ cm cylinder

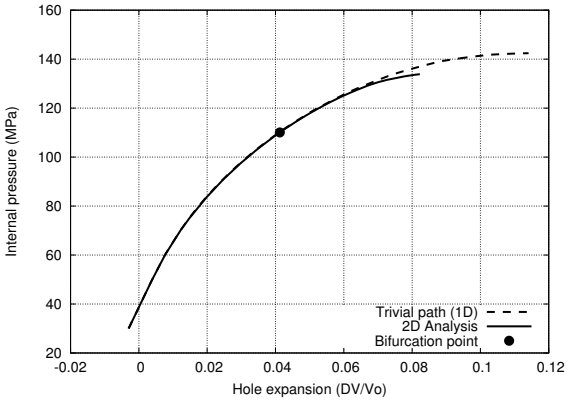

Fig. 6. Internal pressure vs hole expansion for the $R_i = 10$ cm cylinder

terial points are not plotted. As can be seen, the shearbands initiate from the cavity wall and progressively propagate towards the outer boundary. The development of similar, curved shearbands has been observed experimentally in cavity expansion experiments on sand specimens [14]. It should be noted that the hoop stress $\sigma_{\theta\theta}$ remains below the material tensile strength, excluding the possibility of tensile failure before shear failure.

The corresponding internal pressure vs hole expansion curve is presented in Fig. 6, where the trivial deformation path is also plotted for comparison. We see that the two curves coincide up to the bifurcation point, where warping becomes possible. Then they slowly separate as axisymmetry is lost, and the curve corresponding to the bifurcated solution levels off at a pressure lower than the limit pressure, to which the trivial path asymptotically tends. The non-axisymmetric mechanism of localised shear failure is thus more critical than the attainment of limit pressure under axisymmetric deformation. From a practical point of view, this result suggests that rupture in cavity pressurisation may occur at lower internal pressure than the limit pressure predicted by classical elastoplasticity, which is used in the interpretation of geotechnical tests or in fracture initiation prediction in weak rock formations.

Finally, we note that the loss of axisymmetry is totally spontaneous. There is no need to perturb the solution with the dominant eigenvector or to introduce imperfect elements. The small round-off error alone, which is present in any numerical calculation, acts like a natural inhomogeneity and suffices to push the solution off the trivial path, to a bifurcated branch that will lead to the final localised pattern. The same observation has also been made in the

case of externally pressurised thick-cylinders [20, 7].

5. Conclusions

Computations with Gradient Elastoplasticity were used to demonstrate that thick-wall cylinders under internal pressurisation may fail due to shear localisation, rather than due to the propagation of tensile fractures or the attainment of limit pressure. Bifurcation analysis shows that, depending on material properties and cylinder size, the pressurised cavity may become unstable and warp. The resulting loss of axisymmetry leads to stress redistribution around the cavity, promoting the formation of a localised failure mechanism in the form of thin, curved shearbands. This failure mechanism is more critical than uniform axisymmetric expansion, and resembles the one already observed for expanding cavities in sand.

Plane strain analyses with Gradient Elastoplasticity are able to capture the inception of the instability and the resulting spontaneous loss of axisymmetry as a matter of course. No special numerical treatment, like perturbation of the solution with the dominant eigenmode or the introduction of imperfections, is needed. In the post-bifurcation regime, the presented numerical scheme allows robust prediction and modelling of the final, localised failure mechanism.

The numerical results presented here provide a mechanism for explaining the discrepancy between theoretical predictions of classical elastoplasticity and experimental evidence from thick-wall cylinders under internal pressure. They also suggest that, during hydraulic fracturing of weak rock formations under insitu conditions, rupture in the form of shearbands may take place during pressurisation of the cavity at pressure levels lower than the limit value predicted by classical plasticity. Following the initial inception of shear failure, fractures may subsequently propagate in tensile mode once the pressurising fluid penetrates into the shearbands.

REFERENCES

[1] Carter, J. P., J. R. Booker, S. K. Yeung. Cavity Expansion in Cohesive Frictional Soils. *Géotechnique*, **36** (1986), 349–358.

[2] Mantaras, F. M., F. Schnaid. Cylindrical Cavity Expansion in Dilatant Cohesive-Frictional Materials. *Géotechnique*, **52** (2002), 337–348.

[3] Economides, M. J., K. G. Nolte. Reservoir Stimulation, 3rd edition, John Wiley and Sons, 2000.

[4] Fjaer, E., R. M. Holt, P. Horsrud, A. M. Raaen, R. Risnes. Petroleum Related Rock Mechanics, Elsevier Science, 2002.

[5] Papanastasiou, P., M. Thiercelin, J. Cook, D. Durban. The Influence of Plastic Yielding on Breakdown Pressure in Hydraulic Fracturing, In: Proceedings of the 35th US Symposium on Rock Mechanics, 281–286 (Eds Daemen and Schultz), University of Nevada, Reno, 5–7 June 1995, Rotterdam, Balkema, 1995.

[6] Zervos, A., P. Papanastasiou, I. Vardoulakis. A Finite Element Displacement Formulation for Gradient Elastoplasticity. *Int. J. Num. Meth. Engng.*, **50** (2001), No. 6, 1369–1388.

[7] Zervos, A., P. Papanastasiou, I. Vardoulakis. Modelling of Localisation and Scale Effect in Thick-Walled Cylinders with Gradient Elastoplasticity. *Int. J. Solids Structures*, **38** (2001), No. 30–31, 5081–5095.

[8] Zervos, A., I. Vardoulakis, P. Papanastasiou. Influence of Nonassociativity on Localization and Failure in Geomechanics Based on Gradient Elastoplasticity. *Int. J. Geomechanics*, **7** (2007), No. 1, 63–74.

[9] Vardoulakis, I., J. Sulem. Bifurcation Analysis in Geomechanics, Blackie Academic and Professional, 1995.

[10] Vardoulakis, I., E. C. Aifantis. A Gradient Flow Theory of Plasticity for Granular Materials. *Acta Mechanica*, **87** (1991), 197–217.

[11] Vardoulakis, I., K. R. Shah, P. Papanastasiou. Modelling of Tool-Rock Shear Interfaces Using Gradient-Dependent Flow Theory of Plasticity. *Int. J. Rock Mech. Min. Sci. & Geomech. Abstr.*, **29** (1992), No. 6, 573–582.

[12] Vardoulakis, I., G. Frantziskonis. Micro-Structure in Kinematic-Hardening Plasticity. *Eur. J. Mech. A/Solids*, **11** (1992), No. 4, 467–486.

[13] Mindlin, R. D. Microstructure in Linear Elasticity. *Arch. Rat. Mech. Anal.*, **10** (1964), 51–78.

[14] Alsiny, A., I. Vardoulakis, A. Drescher. Deformation Localization in Cavity Inflation Experiments on Dry Sand. *Géotechnique*, **42** (1992), 395–410.

[15] Papanastasiou, P., I. Vardoulakis. Bifurcation Analysis of Deep Boreholes: II. Scale effect. *Int. J. Num. Anal. Meth. Geomech.*, **13** (1989), 183–198.

[16] Vardoulakis, I., P. Papanastasiou. Bifurcation Analysis of Deep Boreholes: I. Surface Instabilities. *Int. J. Num. Anal. Meth. Geomech.*, **12** (1988), 379–399.

[17] Papamichos, E., P. van den Hoek. Size Dependency of Castlegate and Berea Sandstone Hollow-Cylinder Strength on the Basis of Bifurcation Theory, In: Proc. 35th US Symp. Rock Mechanics, 1995, 301–306.

[18] Argyris, J. H., I. Fried, D. W. Scharpf. The TUBA Family of Plate Elements for the Matrix Displacement Method. *The Aeronautical Journal of the Royal Aeronautical Society*, **72** (1968), 701–709.

[19] Dasgupta, S., D. Sengupta. A Higher-Order Triangular Plate Bending Element Revisited. *Int. J. Num. Meth. Engng*, **30** (1990), 419–430.

[20] Papanastasiou, P., I. Vardoulakis. Numerical Treatment of Progressive Localization in Relation to Borehole Stability. *Int. J. Num. Anal. Meth. Geomech.*, **16** (1992), 389–424.